

Stopping and straggling of H and He in ZnO

Raul C. Fadanelli¹, Chiara D. Nascimento¹, Claudia C. Montanari^{2,a}, Julio C. Aguiar³, Dario Mitnik², Andrzej Turos^{4,5}, Elzbieta Guzewicz⁶, and Moni Behar¹

¹ Laboratório de Implantação Iônica, Instituto de Física, Universidade Federal do Rio Grande do Sul, Av. Bento Gonçalves 9500, 91501-970 Porto Alegre, Brazil

² Instituto de Astronomía y Física del Espacio (CONICET-UBA), and Departamento de Física, Facultad de Ciencias Exactas y Naturales, Universidad de Buenos Aires, casilla de correo 67, Sucursal 28, C1428EGA Buenos Aires, Argentina

³ Autoridad Regulatoria Nuclear, Av. Libertador 8250, C1429BNP Buenos Aires, Argentina

⁴ Institute of Electronic Materials Technology, Wólczyńska 133, 01-919 Warsaw, Poland

⁵ National Centre for Nuclear Research, Soltana 7, 04-500 Otwock, Poland

⁶ Institute of Physics, Polish Academy of Sciences, Al. Lotników 32/46, 02-668 Warsaw, Poland

Received 08 March 2016 / Received in final form 04 May 2016

Published online (Inserted Later) – © EDP Sciences, Società Italiana di Fisica, Springer-Verlag 2016

Abstract. We present experimental and theoretical values for the energy loss of H and He ions in Zinc oxide, in mean value (stopping per unit path length) and mean square value (energy loss straggling). The measurements were carried out using the Rutherford Backscattering technique for (300–2000) keV H ions and (300–5000) keV He ions. Present experimental data are the first set of stopping and straggling values in this oxide. The theoretical research was encouraged considering the molecular description of ZnO as crystal solid using the density functional theory. The energy loss calculations for H and He ions with different charge states were performed with the shelwise local plasma approximation (SLPA). The molecular vs the Bragg-rule description is also discussed. The equilibrium charge state of He inside ZnO is analyzed based on the present stopping measurements, and a semiempirical charge state distribution is proposed. Present experimental and theoretical values show good agreement for both the stopping and the straggling. We also compare our data with the SRIM2013 and with CasP5.2 values.

1 Introduction

In recent years, the wide gap semiconductors, including ZnO, GaN and SiC, are revolutionizing numerous areas of developments due to their application in energy-efficient and environmentally friendly devices, from UV/blue light-emitting diodes (LED), sensors, photodetectors, to laser diodes, energy conversion, photovoltaics, communications, biotechnology, imaging, and medicine [1]. Currently the interest, especially in ZnO, is mainly due to the industrial demand. Some compounds based on ZnO are considered as promising fast scintillators [2], with a high radiation hardness and appropriate stopping power. For example, the ZnO:Zn scintillators containing Li have been developed for high-counting rate neutron imaging (see [1] and references therein). The aluminum doped ZnO on polymer foil is also applied in organic solar cell devices [3].

The interest in ZnO is not only based on its new technological applications, but also on the fact that ZnO has been a common material produced commercially at rather low cost for more than a century. Zinc oxide is available mostly in powder or thin film form and only recently a small single crystal ZnO has been produced [4]. In the

wurtzite crystallize structure, ZnO is a direct band gap semiconductor with a band gap of 3.44 eV [5]. In a very recent letter [6] an all-optical experimental technique is presented and applied on a ZnO crystal to reconstruct the momentum-dependent band gaps.

Despite the extensive research described above, some basic properties of this material have not been established so far. Among them are the stopping power and straggling of light ions in the keV-MeV energy range. In turn these quantities are fundamental for the interpretation of the Rutherford Backscattering (RBS) results, which is one of the most used techniques for the thin film analysis. Moreover, it should be stated that no measurement on ZnO target is present in the exhaustive collection of stopping data by Paul [7,8]. Therefore, in this contribution we report the first set of experimental data of energy loss of H and He in ZnO, including stopping power and straggling.

The present data was measured using the RBS technique at the facility of the Instituto de Física, at the Universidade Federal do Rio Grande do Sul, Brazil. This research contributes to the study of the energy loss of ions in different oxides of interest, such as the widely measured Al₂O₃ [9,10], but also HfO₂ [11,12], ZrO₂ [13,14], TiO₂ [15] and Ta₂O₅ [16], for which no previous experimental data were available in the literature.

^a e-mail: claudia.montanari@gmail.com

The theoretical description of the energy loss in complex targets is scarce. The MELF-GOS model is an interesting possibility if reliable measurements of the energy loss function in the optical limit are available [10–16]. In relation to the atomic values, in 1905 Bragg and Kleeman [17] predicted that the stopping power of a compound should be given by the linear combination of the different constituents. This well-known Bragg additivity rule is still employed, not only for stopping power, but also for ionization cross sections, considering the single atomic elements or the small molecular fragments of large molecules such as the nucleobases [18]. Deviations at intermediate and low energies occur mainly because of differences in the electronic structure of the outer shells, where molecular bonds start to become important [19]. A step forward is the core-and-bond approximation (CAB), where the core and outer electron contributions are separately considered [20]. The CAB approximation together with the stopping power data on an important amount of compounds is considered in the SRIM code to deal with stopping in compounds [21].

In this work we face the theoretical challenge of performing ab-initio stopping power calculations using the full molecular description of the ZnO in the solid phase. We use the shellwise local plasma approximation (SLPA) [22–24] together with the density functional theory (DFT) for the ZnO molecules as crystalline solid. This procedure has already been applied successfully in a previous work for TiO₂ target [15].

The SLPA is a many electron model that can be adapted perfectly to complex targets. Its inputs are the electronic densities and binding energies, so as far as a reliable molecular description of the ground state is available, the combination with the SLPA is straightforward. It should also be mentioned that the SLPA deals with atoms or molecules with the same degree of computational effort.

This paper is organized as follows. First, in Sections 2 and 3 we describe the experimental techniques for the sample preparation, the RBS measurements and the data analysis. Details about the SLPA and the DFT calculations are given in Section 4. Afterwards, in Section 5 the present experimental data and the theoretical results for stopping and straggling of H and He in ZnO are presented and discussed, including an empirical estimation of the equilibrium charge state of He inside the ZnO. Finally, the conclusions are summarized in Section 6.

2 Sample preparation and characterization

ZnO films were grown by Atomic Layer deposition (ALD) at the Institute of Physics, Polish Academy of Science, Warsaw. The growth processes were performed using the Savannah-100 reactor from Cambridge NanoTech. Diethylzinc (DEZn) as a zinc precursor and deionized water (DW) as an oxygen precursor were used, while nitrogen was applied as the purging gas. All films were grown at a constant growth rate of 0.07 nm/cycle.

Extensive sample characterization is essential for reliable stopping power measurements. In a large number of

experiments performed to the date polycrystalline samples were used. This requires thorough analysis of crystallite size and their mutual orientation. It should be mentioned that the rolling texture, typically present in metallic foils, has been a source of important systematic errors in a number of stopping power measurements.

Structural characterization was performed using X-ray diffraction and AFM analysis. XRD measurements were performed at the Institute of Electronic Materials Technology, Warsaw, using the Siemens D500 powder diffractometer, equipped with a high-resolution semiconductor Si:Li detector and using K_{α12}Cu radiation ($\lambda = 1.5418$ Å). The diffraction pattern was measured in a $(\theta - 2^\circ)/2\theta$ scanning mode, with a step of 0.05° , counting time of 4 s/step and 2θ range 25° – 65° . The deviation of the specimen surface with two degrees of Bragg-Brentano geometry was done in order to attenuate strong reflections from the single crystal substrate. The experimental data were analyzed by the XRAYAN phase analysis program and ICDD PDF4+ 2013 database package of diffraction standards.

X-ray diffraction profiles revealed the presence of the Si 004 reflection due to the scattering by the substrate and three orders of magnitude lower ZnO 00.2 reflexion. The presence of the latter indicates that the films are of polycrystalline structure. The average crystallite size of about 25 nm has been estimated. This means the produced layers are nanocrystalline and what is very important no texture has been detected. Very low background level in diffraction profiles indicates negligible contribution of the amorphous phase. The results of the present experiments give place to the following thickness of films: $t = 22, 44, 66, 104, 113$ and 172 nm. The typical errors are less than 5%.

AFM measurements revealed that all the films are atomically flat with the Root Mean Square (RMS) of the surface roughness varied between 0.8 nm for the thinnest film (22 nm) to 1.6 nm for the thickest one (172 nm). These results are crucial for the straggling measurements. The detailed description of sample analysis can be found elsewhere [25]. The stoichiometry of the films were checked and confirmed by using the RBS spectrometry.

3 The RBS measurements

3.1 Stopping power

The energy losses of H and He were determined by means of the RBS technique using the ions beams provided by the 3 MV Tandetron of the Instituto de Fisica, Universidade Federal do Rio Grande do Sul. For the H and He beams, the interval of energy covered by the present experiment was between 300 and 3000 keV and the combined electronic plus detector resolution were of 8 and 12 keV (FWHM) respectively. The samples were mounted on a goniometer and the detector was fixed at 120° with respect to the beam direction. For each incident energy, the angle between the beam and the normal to the sample was changed between 0° and 60° . The selection of the sample

1 thicknesses was done according to the beam energy. In
 2 some cases two different samples were analyzed with the
 3 same energy and the results were quite consistent with
 4 each other.

5 The stopping power dE/dx can be obtained from the
 6 experimental data for the ions backscattered at a depth
 7 x of the film, through the following relation based on the
 8 mean energy approximation [26]

$$\Delta E(x) = \frac{K x}{\cos \theta_1} \left. \frac{dE}{dx} \right|_{\overline{E}_{in}} + \frac{x}{\cos \theta_2} \left. \frac{dE}{dx} \right|_{\overline{E}_{out}}, \quad (1)$$

9 where ΔE is the difference between the beam energy at the
 10 surface (E_0) and at the depth x , K is the kinematic factor,
 11 θ_1 (θ_2) is the angle between the sample normal and the
 12 incoming beam (the detector direction), and $dE/dx|_{\overline{E}_j}$ is
 13 the stopping power at the energy \overline{E}_j .

14 Considering (1) for ions backscattered at the back of
 15 the ZnO film, x equals the film thickness Δx . When mea-
 16 suring ΔE (the difference between E_0 and the energy at
 17 the back signal edge) at two or more different geometries,
 18 a system of equations is obtained which allows to
 19 get the stopping values $dE/dx|_{\overline{E}_{in}}$ and $dE/dx|_{\overline{E}_{out}}$. For
 20 each energy, four measurements were taken under differ-
 21 ent geometrical conditions ($\theta_1 = 0^\circ, 20^\circ, 40^\circ$ and 60°
 22 $\theta_2 = 60^\circ - \theta_1$). The energies \overline{E}_{in} and \overline{E}_{out} were taken as
 23 the mean values of the values obtained via mean energy
 24 approximation [26]. Proceeding in the same way for each
 25 energy, the stopping powers of ZnO for H and He were
 26 obtained. See reference [12] for further details.

27 3.2 Straggling

28 The ion beams were provided by the 3 MV Tandetron,
 29 with incident energies covering a wide range. For H ions
 30 it was from 300 up to 1500 keV, while for He ions it was
 31 from 300 up to 3000 keV. For each incident beam and
 32 energy we have used an appropriate film. In each case we
 33 have recorded three spectra at $0^\circ, 30^\circ$ and 45° between
 34 the normal of the sample and the incident ion beam. This
 35 procedure was followed in order to improve the present
 36 results precision.

37 In Figure 1 we show a 1 MeV RBS signal of Zn be-
 38 longing to a 172 nm ZnO film tilted at 30° with respect to
 39 the sample normal. The fits to the Zn signal are displayed
 40 with full lines. Following the procedure related in [11] and
 41 taking into account the RMS natural roughness we were
 42 able to obtain the straggling corresponding to each mea-
 43 sured sample and measured energy.

44 4 Theoretical model

45 Our theoretical developments lay over two complemen-
 46 tary models, the SLPA for the energy loss [22–24] (briefly
 47 summarized in Sect. 4.1) and the DFT applied to de-
 48 scribe the ZnO in the crystalline solid face (described in
 49 Sect. 4.2).

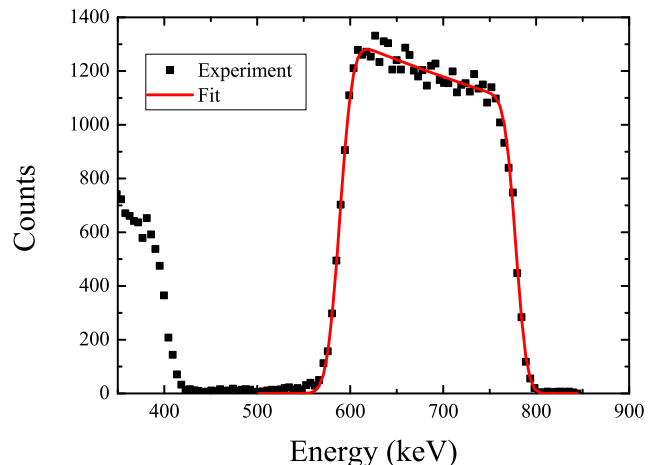


Fig. 1. RBS spectrum for 1 MeV He in ZnO. The symbols stand for the experimental spectrum. The line is a fit to the ZnO signal.

4.1 SLPA for the energy loss

50 We modeled the inelastic processes that take place when
 51 H or He ions interact with the ZnO electrons by using the
 52 SLPA [22]. This approximation works within the dielectric
 53 formalism describing the response of the bound electrons
 54 as a local electron gas with an ionization gap using Levine-
 55 Louie dielectric function for each subshell [27]. The SLPA
 56 is not an independent particle approximation, it includes
 57 single and collective processes, the dynamic screening of
 58 the projectile charge, and the electron correlation in the
 59 final state. The main limitation is that it is a perturbative
 60 formalism, valid for asymmetric collisions and high ener-
 61 gies, i.e. $Z_P < Z_T$, and $Z_P/v < 1$, with Z_P (Z_T) being the
 62 projectile (target) nuclear charge and v the impact veloc-
 63 ity. In addition, it is an impulse type approximation [28]
 64 and assumes that the time of response of target electrons
 65 is larger than the collision time, i.e. the ion impact veloc-
 66 ity larger than the mean velocity of the bound electrons.
 67 Within this frame, the SLPA probed to describe the dif-
 68 ferent energy loss moments, such as the ionization cross
 69 sections [29–32], the stopping power [23,24,33] and the
 70 energy loss straggling [34,35], in good agreement with the
 71 measurements.

72 Considering the inelastic collisions of the ion and the
 73 cloud of target electrons with binding energy E_{nl} and local
 74 density $\rho_{nl}(\mathbf{r})$, the SLPA expression for the energy loss
 75 moment of order t ($t = 0$ for the ionization cross section,
 76 $t = 1$ for the stopping power, $t = 2$ for the square energy
 77 loss straggling) is given by

$$S_{nl}^{(t)} = \frac{2}{\pi v^2} \int_0^\infty \frac{[Z_P(k)]^2}{k} dk \int_0^{kv} \omega^t \text{Im} \left[\frac{-1}{\varepsilon_{nl}(k, \omega)} \right] d\omega, \quad (2)$$

with

$$\text{Im} \left[\frac{-1}{\varepsilon_{nl}(k, \omega)} \right] = \int \text{Im} \left[\frac{-1}{\varepsilon^{LL}(k, \omega, \rho_{nl}(\mathbf{r}), E_{nl})} \right] d\mathbf{r}, \quad (3)$$

50

51

52

53

54

55

56

57

58

59

60

61

62

63

64

65

66

67

68

69

70

71

72

73

74

75

76

77

78

79

1 and with $\varepsilon^{LL}(k, \omega, \rho_{nl}, E_{nl})$ being the Levine-Louie dielectric
 2 function [27]. The importance of using this dielectric
 3 function is the explicit inclusion of the binding energies.
 4 The total energy loss moment will be the addition of the
 5 shell to shell contributions, $S^{(t)} = \sum_{nl} S_{nl}^{(t)}$. More details
 6 about the SLPA can be found in [36], and a review on this
 7 approximation in [22].

8 We include the ion charge state in (2) as $Z_P(k)$ to take
 9 into account the dressed ions (i.e. He^0 and He^+) and the
 10 screened nuclear charge. Note that this is not a constant
 11 effective charge. It is calculated considering the wave func-
 12 tions of the ion bound electrons using Hartree-Fock tables
 13 for neutral and for positive ions by Clementti-Roetti [37],
 14 and transformed to the momentum space. For bare ions it
 15 is just Z_P . An analytical fitting of the exact values for ions
 16 He^{+q} to Ne^{+q} can be found in [22] together with tables
 17 for the different ions.

18 When the ion travels inside the solid, ionization and
 19 capture processes take place leading to an equilibrium
 20 charge state, which depends on the ion velocity. At high
 21 energies, electron loss prevails over capture and the ion
 22 ends stripped from bound electrons. We performed the
 23 SLPA calculations for the different possible equilibrium
 24 charge states of the ion by using (2) and (3). In this equi-
 25 librium regime (many collisions inside the bulk), the total
 26 stopping can be approximated as

$$S_{total}^{(t)} = \sum_{q=0}^{Z_P} f_q(v) S^{(t)}, \quad (4)$$

27 with $f_q(v)$ being the charge fraction of H^{+q} ($q = 0, 1$) or
 28 He^{+q} ($q = 0, 1, 2$). The mean charge state is $q_{mean}(v) =$
 29 $\sum_q q f_q(v)$.

30 Total stopping power calculations are very sensitive to
 31 these values. In some cases experimental values are avail-
 32 able. Well-known fittings of the experimental mean charge
 33 states are those by Grande and Schiwietz [38], and by
 34 Ziegler et al. [39] (included in the SRIM code [21]). Both
 35 proposals, while different, show good descriptions of the
 36 stopping cross sections tested on an extended ion-target
 37 sampling. However, measurements of equilibrium charge
 38 states for the different projectile-target combinations, in-
 39 cluding compounds, are still necessary. Particularly, there
 40 are no experimental values on Zn or ZnO. Experiment-
 41 al and theoretical works are still focused on this sub-
 42 ject [40–45] due to the relevance of reliable values of the
 43 charge state distributions of ions through matter. We will
 44 return to this point in Section 5.2.

45 4.2 DFT for ZnO

46 We resort to the density functional theory (DFT) to ob-
 47 tain the ZnO electronic density, the binding energies,
 48 the cohesive energy, and the band structure. The rad-
 49 ial wave functions of the core electrons, the pseudo-
 50 potentials and the pseudo-atomic orbitals of the valence
 51 electrons were generated by means of the ADPACK

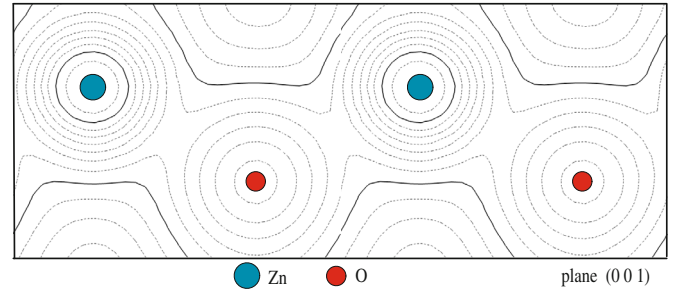


Fig. 2. The wurtzite crystal structure electron density.

and OpenMX codes. These codes solve numerically the
 non-relativistic Kohn-Sham equations under the general-
 ized gradient approximation (GGA) with a Troullier and
 Martins scheme [46], and following the developments of
 Perdew, Burke and Ernzerhof [47], also known as GGA-
 PBE. The calculations were carried out for the $\text{Zn}^{2+}\text{-O}^{2-}$
 configuration, i.e. the valence band O-2p completely filled.
 A similar procedure was introduced in [15] for TiO_2 .

We assumed ZnO to be hexagonal zincite in space
 group 186 with Hermann Mauguin notation P63/mc [48]
 (see Fig. 2). The lattice constants were determined by
 energy minimization per molecule. We obtained $a = 3.29$ Å
 and $c = 5.40$ Å, very close to the experimental values
 $a = 3.2495$ Å and $c = 5.2069$ Å [48]. We also calculate the
 cohesive energy of ZnO, -6.85 eV, while the experimen-
 tal one is -7.52 eV (deduced from experimental Zn heat
 vaporization, ZnO enthalpy of formation, and O2 bind-
 ing energy for the wurtzite phase [49]). Some authors [50]
 consider that the DFT-GGA severely underestimates the
 gap. This is not the case for present calculations. We ob-
 tain a band-gap of 3.65 eV, where experimental value is
 3.44 eV at low temperatures and 3.37 eV at room tem-
 perature [51,52]. This value is rather good, though 7%
 above the experimental value. Present results for the band
 structure of ZnO using DFT-GGA-PBE calculations are
 displayed in Figure 3.

The binding energies of the target electrons are impor-
 tant inputs for the SLPA calculations. Present DFT-GGA
 results for the ZnO valence electrons (in atomic units) are
 $E_{2p} = -0.355$ for the O^{2-} and $E_{3d} = -0.395$ for the
 Zn^{2+} . These energies are around half of the corresponding
 atomic ones ($E_{2p} = -0.632$ and $E_{3d} = -0.783$ [37]). This
 is interesting because the SLPA describes the response of
 the ZnO valence shell as separate clouds of the six O-2p
 electrons and the ten Zn-3d electrons, with rather similar
 binding energies and mean velocity around 0.9 a.u. The
 contribution of these subshells is very important at the
 energies of the stopping maximum. We will return on this
 point in Section 5.2.

The other input for the SLPA is the target elec-
 tronic density. The quality of the DFT-GGA-PBE can
 be verified by comparing the calculated electronic den-
 sity with the experiments of Compton scattering [53]. In a
 non-relativistic and high-energy transfer regime, theoret-
 ical calculations for isotropic Compton profiles are com-
 monly performed under the impulse approximation. It is

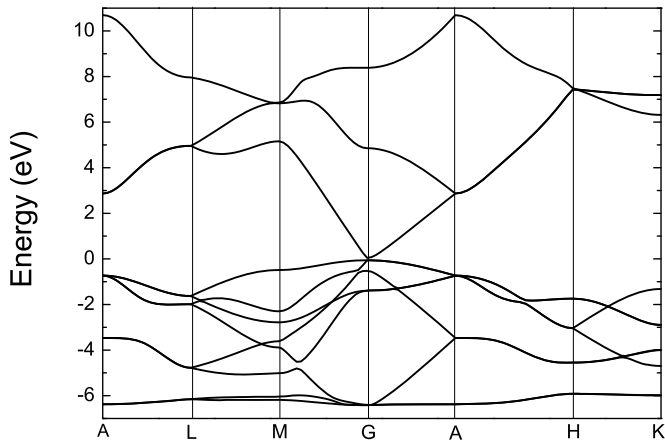


Fig. 3. Band structure calculation of ZnO using GGA-PBE functional.

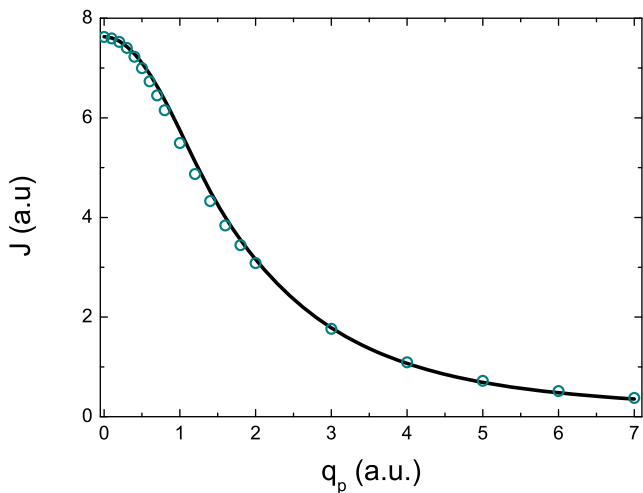


Fig. 4. Compton profile of ZnO. The solid curve indicates the present DFT-GGA calculation, whereas the circles are the experimental data from reference [53].

1 assumed that energy and momentum are conserved. This
2 approach is expected to be valid when the energy trans-
3 ferred in the scattering process is much greater than the
4 binding energy of the electron orbital [54].

5 The isotropic Compton profile (in atomic units) under
6 the impulse approximation, is defined as:

$$J(q_p) = \frac{1}{2} \int_{q_p}^{\infty} n(p) p dp, \quad (5)$$

7 where $n(p)$ is electron momentum density related to the
8 square of the Fourier transform of the radial wave func-
9 tion, p is the electron linear momentum before the collision
10 (in module), and q_p is the projection of the momentum
11 transfer on the direction of \vec{p} .

12 Present DFT-GGA-PBE results for the Compton
13 profile of crystalline ZnO are compared with Kumar
14 et al. [53] measurements in Figure 4, showing a very good

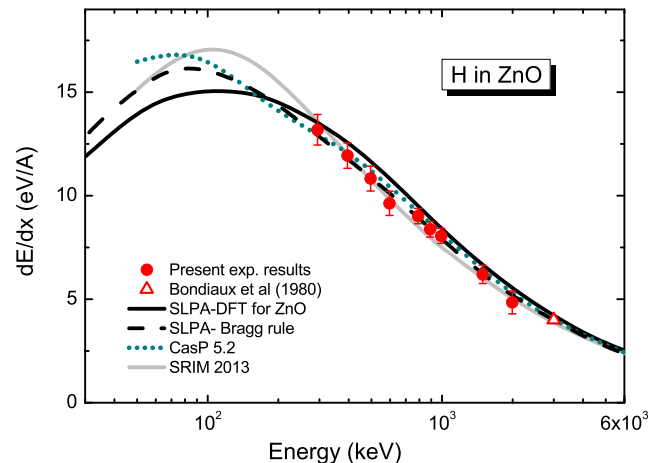


Fig. 5. Stopping power of ZnO for protons. Symbols: filled circles, present data; hollow triangle, [56]. Curves: solid line, present SLPA calculations with DFT molecular values for ZnO; dashed-line, SLPA for ZnO using Bragg rule (atomic Zn and O); dotted-line Casp5.2 values [38,57–59]; grey-solid line, SRIM 2013 values [21].

description of the data. This method has already been
15 tested for TiO₂ [15] with very good agreement too, as
16 noted in reference [55].
17

5 Results and discussion 18

5.1 Stopping and straggling of ZnO for H 19

In Figure 5 we display the present experimental data
20 (filled squares) and the theoretical values (solid curve) for
21 the mean energy loss per unit path length, dE/dx , of H
22 in ZnO bulk. The stopping per unit path length given
23 by reference (4) relates to the stopping cross section per
24 molecule as $S^{(1)}\rho = dE/dx$. In the present case, the den-
25 sity of ZnO molecules is $\rho = 4.148 \times 10^{22}$ molecules/cm³.
26

27 There is only one previous value available in the liter-
28 ature for stopping of H by ZnO by Bondiaux et al. [56], at
29 3 MeV, which is also displayed in Figure 5. The tendency
30 of the present data is in agreement with this value. The
31 SLPA results shown in Figure 5 have been obtained using
32 the DFT-GGA molecular values for ZnO as described in
33 Section 4.1.

34 For impact energies $E \geq 300$ keV, the equilibrium
35 charge state of H is +1, so in the energy range of present
36 experimental data the description of the H⁺-ZnO collision
37 is enough. Following [38], the extension of present SLPA
38 results to energies below 200 keV should consider the pres-
39 ence of H⁰ inside ZnO. In that case, the total stopping
40 of H in ZnO for $E < 200$ keV would be lower than the results
41 shown in Figure 5.

42 We also include in Figure 5 the SLPA calculations
43 using Bragg rule (adding the atomic results for Zn and
44 O), the predictions of the convolution approximation for
45 swift particles (Casp5.2) [57–59], and the semi-empirical

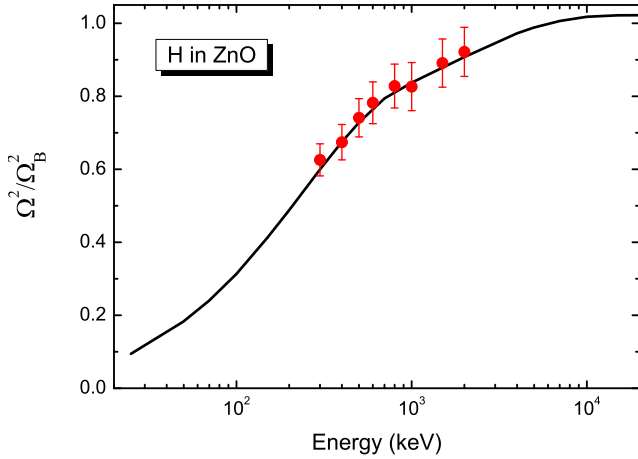


Fig. 6. Square energy loss straggling of H ions in ZnO, normalized to Born value. Symbols: filled circles, present data. Curves: solid line, present SLPA calculations with DFT molecular values for ZnO

1 SRIM2013 values [21]. It is worth to mention that SRIM
2 values for H in solids only consider the +1 charge state.

3 Our full-molecular SLPA-DFT results in Figure 5
4 (solid-line) correctly describe the present experimental
5 values. It is fair to say that also the atomic SLPA results
6 using the Bragg rule (dashed-line) agree quite well with
7 the high energy measurements. The different predictions
8 for the stopping of H in ZnO included in Figure 5 describe
9 the data for $E \geq 300$ keV/amu and differ for lower ener-
10 gies. The differences around the stopping maximum can-
11 not be solved without measurements in this energy region.
12 The SLPA proved to be valid for energies somewhat lower
13 than the stopping maximum [22]. But it is a perturbative
14 approximation, to lower energies the Barkas effect should
15 be estimated [44], or a non-perturbative model should be
16 used.

17 In Figure 6 we display present experimental and
18 theoretical values for the square energy loss straggling
19 per molecule, $\Omega^2 = S_{total}^{(2)}$ given by (4). These val-
20 ues are normalized to Bohr high energy limit $\Omega_B^2 =$
21 $4\pi Z_P^2 Z_T \rho \Delta x$ [60], with ρ being the target density
22 and Δx being the width. The agreement is quite good
23 in the whole experimental energy range. Straggling mea-
24 surements represent a highly demanding test of the sample
25 preparation described in Section 2.

26 5.2 Stopping and straggling of ZnO for He

27 We performed the SLPA calculations for He^0 , He^+ , and
28 He^{+2} using (2) with the corresponding screening functions
29 $Z_P(k)$. In the equilibrium regime the total stopping is ob-
30 tained considering the ion charge state at each impact ve-
31 locity as expressed in (4). Present stopping measurements
32 suggest that the charge state of He in ZnO is close to +2,
33 even at 400 keV/amu. This value is greater than CasP
34 code prediction based on the fitting in [38] for atomic tar-
35 gets and Bragg rule [17].

36 The charge state of fast ions moving through matter
37 fluctuates due to electron loss and capture processes. After
38 a large number of collisions, an equilibrium charge state is
39 reached, which is independent of the ion incident charge
40 state, it only depends on the impact energy and the target.
41 This subject has been extensively studied for ions through
42 gaseous and solid media. Reviews on this can be found
43 in [61] and more recently in [62].

44 A benchmark for the equilibrium charge state is the
45 known Thomas-Fermi (TF) charge, based on Bohr strip-
46 ping criteria [45]

$$q_{eq} = Z_P [1 - \exp(-v/Z_P^{2/3})]. \quad (6)$$

47 More complex theoretical developments are based on TF
48 function [63]. An analytical fitting formula based on this
49 model has been recently given by Sigmund [62] as

$$q_{eq} = Z_P \frac{1 - \exp(-1.43 v/Z_P^{2/3})}{1 + \exp(-3.56 v/Z_P^{2/3})}. \quad (7)$$

50 Empirical fittings for specific ion-target combinations are
51 also available in the literature, [64–66], including a recent
52 two-parameter fitting for heavy ions in different targets by
53 Sagaidak et al. [43]. Of course, all the different ion-target
54 systems cannot be covered. Betz proposal [64] is to fit the
55 measured equilibrium charge as

$$q_{eq} = Z_P [1 - \alpha \exp(-v/Z_P^\gamma)], \quad (8)$$

56 with α and γ being fitting parameters for specific ion-
57 target data. TF model predicts $\gamma = 2/3$, while for To and
58 Drouin it is $\gamma = 0.45$ [65].

59 Perhaps the most accurate proposal of equilibrium
60 charge state of ions in matter is that by Schiwietz and
61 Grande [38], highly probed for different systems and used
62 in stopping power calculations. It is based on a universal
63 scaling (different projectiles and targets) ratified by an
64 important amount of experimental data. This empirical
65 scaling and fitting is employed in CasP code [38] and in
66 many other stopping power calculations [15,23].

67 For compounds many of the semiempirical models use
68 Bragg rule [17] despite the fact that for cases such as ZnO,
69 it is a semiconductor with a clear band gap, while Zn is a
70 metal, and the ratio between loss and capture cross sec-
71 tions is expected to be quite different. In previous cal-
72 culations of stopping of He in oxides [15] we obtain the
73 stopping cross sections using the values of the equilibrium
74 charge fractions at each impact velocity supplied by the
75 CasP code [38]. However, we found experimental evidence
76 of He^{2+} at lower energies than those predicted by [38]. In
77 this contribution we estimate empirically the mean charge
78 state of He inside ZnO as the square root of the ratio of
79 the present He to H stopping measurements,

$$q_{eq} = \sqrt{S(\text{He})/S(\text{H})}. \quad (9)$$

80 This value is also called effective charge [39], and has been
81 extensively used and discussed in stopping power calcula-
82 tions. At high energies the energy loss depends on the ion

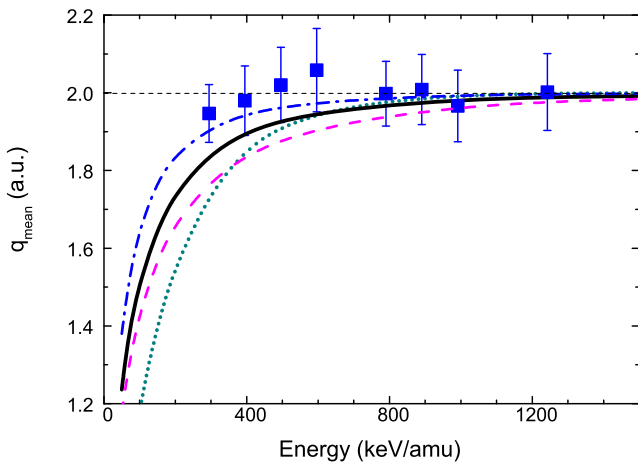


Fig. 7. Mean charged state of He inside ZnO. Symbols: filled squares, present data. Curves: solid line, present semiempirical proposal; dotted-line, Casp values [38]; dashed-line, standard TF expression in (6); dashed-dotted line, Sigmund formula given by (7) [62].

1 charge as Z_P^2 (perturbative regime). Lower values are expected for intermediate to low energies (saturation, non-perturbative regime, presence of He^+ ions). A review on the advantages and failures of the effective charge concept can be found in [45].

2 We decided to evaluate the charge state of He in ZnO
 3 by comparing our stopping measurements for He and H
 4 ions, and calculating the empirical q_{eq} given by (9).
 5 In Figure 7 we display present experimental values for
 6 q_{eq} at ion energies $E \geq 300$ keV/amu. The interesting
 7 point is that it is an insight on the charge state inside
 8 the solid. As expected, at high energies the measured
 9 q_{eq} is close to the nuclear charge, and it is slightly
 10 below +2 for ($300 \leq E \leq 400$) keV/amu. Based on
 11 these results we propose an empirical function for
 12 $q_{eq}(v)$ of He inside solid ZnO, also displayed in
 13 Figure 7 (solid line). This proposal considers the
 14 experimental values for energies $E \geq 400$ keV/amu,
 15 and extend it to lower energies. We take into account
 16 the experimental error in this fitting following the
 17 smallest value for $E \leq 600$ keV/amu. The criteria
 18 was to change the least possible from the universal
 19 scaling by Grande and Schiwietz in [38], also
 20 displayed in Figure 7. Our curve can be fitted by a
 21 Betz type function, given by (8), with $\gamma = 0.45$,
 22 as suggested by To and Drouin [65]. We also include
 23 in Figure 7 the results given by (6) and (7). Of
 24 course, the accuracy of TF theory is expected to be
 25 valid for ions with atomic number larger than 2,
 26 however, the agreement of Sigmund formula (7) with
 27 present measurements in this figure is amazing.

28 In Table 1 we present the numerical results of present
 29 empirical function for He in ZnO. The charge state
 30 fractions f_q were obtained considering that in the
 31 energy range of present experiments only He^{+2} and
 32 He^+ can be found inside the ZnO. It can be noted
 33 that the difference with respect to [38] is only for
 34 energies below 500 keV/amu. We use the values in
 35 Table 1 to obtain the total stopping using (4).
 36
 37

Table 1. Equilibrium charge state of He in ZnO as function of the ion energy (E in keV/amu). Charge fractions f_q (in percentage) and equilibrium charge state q_{eq} (in atomic units) correspond to the fitting in Figure 7. The q_{eq}^{exp} are obtained from the ratio of our stopping measurements as in (9). Also included are the CasP values [38], q_{eq}^{CasP} .

E	f_0	f_1	f_2	q_{eq}	q_{eq}^{exp}	q_{eq}^{CasP}
30	15.0	72.5	12.5	0.97		0.611
50	3.9	68.6	27.5	1.24		0.828
100	0.0	48.9	51.1	1.51		1.19
200	0.0	25.8	74.2	1.74		1.56
300	0.0	15.5	85.5	1.84	1.95 ± 0.07	1.75
400	0.0	10.1	89.9	1.90	1.98 ± 0.09	1.86
500	0.0	7.0	93.0	1.93	2.02 ± 0.10	1.92
600	0.0	5.2	94.8	1.95	2.06 ± 0.10	1.95
800	0.0	2.9	97.1	1.97	2.00 ± 0.08	1.98
900	0.0	2.3	97.7	1.98	2.01 ± 0.09	1.99
1000	0.0	1.8	98.2	1.98	1.97 ± 0.09	1.99
1250	0.0	1.2	98.8	1.98	2.00 ± 0.10	2.00
1500	0.0	0.7	99.3	1.99		2.00
2000	0.0	0.4	99.6	2.00		2.00
5000	0.0	0.0	100	2.00		2.00

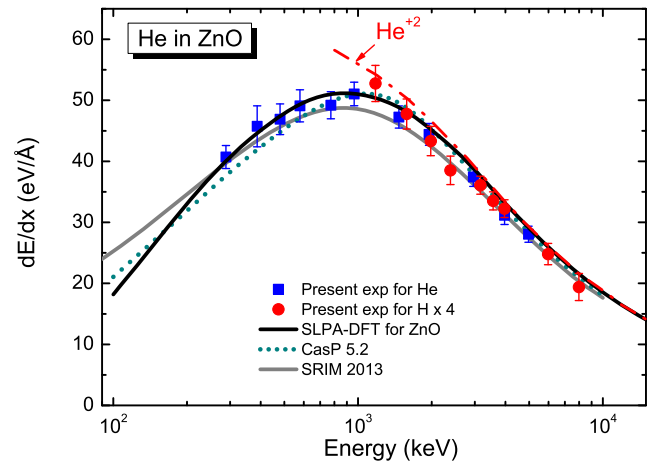


Fig. 8. Stopping power of ZnO for He ions. Symbols: filled squares, present measurements for He ions; filled circles, present data for H ions $\times Z_P^2$. Curves: solid line, present SLPA calculations with DFT molecular values for ZnO; dotted-line Casp5.2 values [38,57–59]; grey-solid line, SRIM 2013 values [21].

38 In Figure 8 we display our experimental data and theoretical results for the stopping power per unit path length of He ions in ZnO. The molecular SLPA calculations for ZnO were performed considering the different He ions (He^0 , He^+ and He^{+2}), and the f_q values displayed in Table 1. Present measurements for He in ZnO cover the stopping maximum. The SLPA results show good agreement with the experimental measurements in the extended (0.3–10) MeV energy region. We also display in this figure the present measurements for H in ZnO $\times 4$. The experimental agreement among He and H $\times Z_P^2$ measurements above 1400 keV is clear, indicating that Barkas contribution
 39
 40
 41
 42
 43
 44
 45
 46
 47
 48
 49

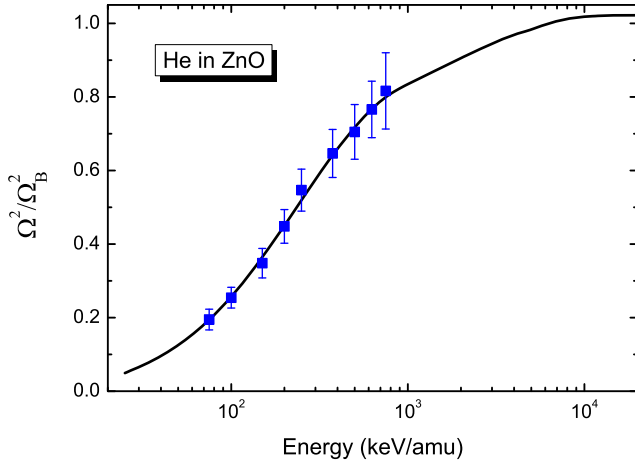


Fig. 9. Square energy loss straggling of He ions in ZnO, normalized to the Born value. Symbols: filled squares, present data. Curves: solid line, present SLPA calculations with DFT molecular values for ZnO; grey dashed dotted-line, similar calculation only for He^{+2} ions.

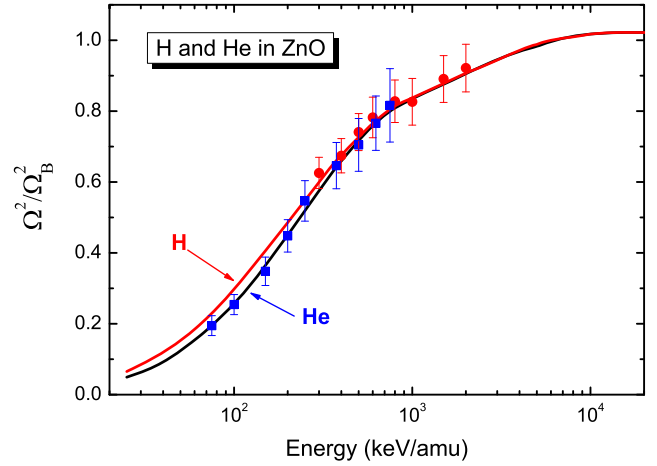


Fig. 10. Square energy loss straggling of H and He in ZnO, normalized to the Born value. Symbols: grey hollow-squares, present data for H ions, black filled-squares, present data for He ions. Curves: black solid line, present SLPA-DFT values for He in ZnO; grey solid-line present SLPA-DFT calculations for H in ZnO

1 (Z^3 dependence) is negligible in this region. These data
 2 also agree quite well with the SLPA results for He^{+2} shown
 3 in Figure 8. The difference between this He^{+2} curve and
 4 the total one is due to the He^{+1} and He^0 ions at interme-
 5 diate and low energies.

6 Also in Figure 8 are the predictions by the CasP5.2
 7 code [38,57–59] (binary collisional model, includes Barkas
 8 contribution) and by the SRIM2013 algorithm [21]. The
 9 different descriptions agree rather well with the new data,
 10 with the SRIM values being somewhat low, but within the
 11 experimental error. The SLPA and the CasP5.2 curves are
 12 together above 1 MeV, below 600 keV the SLPA shows a
 13 better description of the experimental data. In this energy
 14 region the response of the valence electrons is decisive. We
 15 found that the ZnO outer electrons ($2p$ of O^{-2} and $3d$ of
 16 Zn^{+2}) are the main contribution to the stopping power for
 17 He impact energies up to 2 MeV. This covers the stopping
 18 maximum, reinforcing the DFT description of the ZnO
 19 molecule and its binding energies, as mentioned in Sec-
 20 tion 4.2. The SLPA-experimental agreement displayed in
 21 Figure 8 is quite good down to 300 keV, feature that can
 22 be assigned to the collective character of the theoretical
 23 treatment. The presence of dressed ions (He^0 and He^+)
 24 and the dynamic screening of the ion by the target elec-
 25 trons (collective response) reduce the effective potential
 26 and expand the validity of our perturbative approach. For
 27 lower energies, the contributions of higher perturbative
 28 orders such as the Barkas-Andersen effect are important.
 29 However, this effect is not straightforwardly quantified for
 30 dressed ions [44].

31 Present measurements and calculations for the square
 32 energy loss straggling are displayed in Figure 9. The full
 33 SLPA calculation, considering the charge states of He in
 34 ZnO given in Table 1, is in very good agreement with the
 35 present data. This is a second test for our proposal.

36 The square energy loss straggling normalized to Bohr
 37 ($\Omega_B^2 \propto Z_P^2$) is almost insensitive to the ion charge (at least

for low charged ions and intermediate to high energies). In
 Figure 10 we plotted together the experimental and theo-
 retical values for the energy loss straggling in ZnO for H
 and He ions. We can note that the measurements for H
 and He in ZnO are quite close above 300 keV/amu. This
 is the expected behavior and reinforces present measure-
 ments of the energy loss straggling.

6 Conclusions

In this work we present a theoretical-experimental study
 of the stopping and straggling of H and He ions into ZnO
 matrix. The theoretical approach is based on the SLPA
 formalism, with DFT to describe the ZnO crystal; while
 the experiments were realized using the RBS technique.
 The theoretical-experimental agreement for the stopping
 power values is quite good. In the particular case of the
 He data, they reproduce very well the predicted maxi-
 mum stopping power, feature that is not easy to achieve.
 It would be worthwhile to mention that the theoretical
 results are in general very sensitive to the charge state of
 the ions inside the matrix. In the present case we have
 considered H^+ for the H ions in view of their high velocity
 inside the ZnO sample. This is not the case for He where
 He^0 , He^+ and He^{+2} contribute to the stopping power. We
 give a semiempirical proposal for the charge states of He
 inside ZnO bulk based on present measurements of the
 stopping power. Down to 500 keV the present and the
 CASP predictions concerning the mean charge agree, how-
 ever for lower energies there is a small difference, which
 strongly reflects on the stopping power results. At vari-
 ance, the straggling results are not too much sensitive to
 the charge state. The theoretical-experimental agreement
 for the energy loss straggling is very good for both, H and
 He impact.

1 In memory of Helmut Paul, whose scientific contributions and
 2 compilation of data on stopping power have been of great im-
 3 portance to our community. The authors thank Prof. Jorge
 4 Miraglia for useful comments. The following institutions finan-
 5 cially support this research: in Brazil the CNPq by the con-
 6 tract PDJ 500314 2014/4; in Argentina, the CONICET by the
 7 PIP2014-2016, the ANPCyT PICT 2014-2363, and the Uni-
 8 versity of Buenos Aires by the projects UBACyT 20020130100
 9 632BA and 20020130100 477BA.

10 References

- 11 1. *Handbook of Zinc Oxide and Related Materials*, edited by
 12 Z.C. Feng (CRC Press, Taylor and Francis Group), Vol. II,
 13 pp. 435-484
- 14 2. V.A. Demidenko E.I. Gorokhova, I.V. Khodyuk, O.A.
 15 Khristich, S.B. Mikhlin, P.A. Rodnyi, *Radiat. Meas.* **42**, 549
 16 (2007)
- 17 3. M. Dosmailov, L.N. Leonat, J. Patek, D. Roth, P. Bauer,
 18 M.C. Scharber, N.S. Sariciftci, J.D. Pedarniga, *Thin Solid*
 19 *Films* **591**, 97104 (2015)
- 20 4. P.J. Simpson, R. Tjossem, A.W. Hunt, K.G. Lynn , V.
 21 Munné, *Nucl. Instrum. Meth. Phys. Res. A* **505**, 82 (2003)
- 22 5. H. Morkoc, U. Özgür, *Zinc Oxide, Fundamental, Materials*
 23 *and Device Technology* (Wiley-VCH Verlag GmbH&Co
 24 KGaA, Weinheim, 2009), Chap. 1
- 25 6. G. Vampa, T.J. Hammond, N. Thiré, B.E. Schmidt,
 26 F. Légaré, C.R. McDonald, T. Brabec, D.D. Klug, P.B.
 27 Corkum, *Phys. Rev. Lett.* **115**, 193603 (2015)
- 28 7. H. Paul, *Stopping Power for Light Ions*. [https://www-nds.](https://www-nds.iaea.org/stopping/)
 29 [iaea.org/stopping/](https://www-nds.iaea.org/stopping/)
- 30 8. H. Paul, A. Schinner, *Nucl. Instrum. Meth. Phys. Res. B*
 31 **227**, 461 (2005)
- 32 9. E.D. Cantero et al., *Nucl. Instrum. Meth. Phys. Res. B* **287**,
 33 1 (2012)
- 34 10. M. Behar, R.C. Fadanelli, L.C.C.M. Nagamine, E.D.
 35 Cantero, G.H. Lantschner, J.C.Eckardt, N.R. Arista, C. D
 36 Nascimento, R. Garcia-Molina, I. Abril, *Eur. Phys. J. D* **68**,
 37 194 (2014)
- 38 11. I. Abril, M. Behar, R. Garcia-Molina, R.C. Fadanelli,
 39 L.C.C.M. Nagamine, P.L. Grande, L. Schünemann, C.D.
 40 Denton, N.R. Arista, E.B. Saitovitch, *Eur. Phys. J. D* **54**,
 41 65 (2009)
- 42 12. M. Behar, R.C. Fadanelli, I. Abril, R. Garcia-Molina, C.D.
 43 Denton, L.C.C.M. Nagamine, N.R. Arista, *Phys. Rev. A* **80**,
 44 062901 (2009)
- 45 13. M. Behar, R.C. Fadanelli, I. Abril, R. Garcia-Molina,
 46 L.C.C.M. Nagamine, *Eur. Phys. J. D* **64**, 297 (2011)
- 47 14. M. Behar, C.D. Denton, R.C. Fadanelli, I. Abril, E.D.
 48 Cantero, R. Garcia-Molina, and L.C.C.M. Nagamine, *Eur.*
 49 *Phys. J. D* **59**, 209 (2010)
- 50 15. S.P. Limandri, R.C. Fadanelli, M. Behar, L.C.C.M.
 51 Nagamine, J.M. Fernández-Varea, I. Abril, R. Garcia-
 52 Molina, C. C. Montanari, J.C. Aguiar, D. Mitnik, J.E.
 53 Miraglia, N.R. Arista, *Eur. Phys. J. D* **68**, 194 (2014)
- 54 16. R.C. Fadanelli, M. Behar, L.C.C.M. Nagamine, M. Vos,
 55 N.R. Arista, C.D Nascimento, R. Garcia-Molina, I. Abril, *J.*
 56 *Phys. Chem. C* **119**, 20561 (2015)
- 57 17. W.H. Bragg, R. Kleeman, *Philos. Mag.* **10**, 318 (1905)
- 58 18. S. Paredes, C. Illescas, L. Méndez, *Eur. Phys. J. D* **69**, 178
 59 (2015)
19. L.N. Trujillo-L ópez, C. Martínez-Flores, R. Cabrera-
 Trujillo, *Nucl. Instrum. Meth. Phys. Res. B* **336**, 130 (2014)
20. H. Paul, A. Schinner, *Nucl. Instrum. Meth. Phys. Res. B*
249, 15 (2006)
21. J.F. Ziegler, J.M. Manoyan, *Nucl. Instrum. Meth. Phys.*
Res. B **35**, 215 (1988). SRIM code, <http://www.srim.org/>
22. C.C. Montanari, J.E. Miraglia, *Theory of Heavy Ion*
Collision Physics in Hadron Therapy, in *Advances in*
Quantum Chemistry, edited by Dz. Belkic (Elsevier,
 Amsterdam, 2013), Chap. 7, pp. 165-201.
23. E.D. Cantero, R.C. Fadanelli, C.C. Montanari, M. Behar,
 J.C. Eckardt, G.H. Lantschner, J.E. Miraglia, N.R. Arista,
Phys. Rev. A **79**, 042904 (2009)
24. C.C. Montanari, C.D. Archubi, D.M. Mitnik, J.E.
 Miraglia, *Phys. Rev. A* **79**, 032903 (2009)
25. A. Turos, E. Guzewicz, A. Stonert, D. Snigurenko, B.S.
 Witkowski, R. Diduszko, M. Behar, *Quasi-amorphous zinc*
oxide layers produced by Atomic Layer Deposition, pss(a)
 submitted (2016).
26. W.K. Chu, J.W. Mayer, M.A. Nicolet, *Backscattering*
Spectrometry (Academic, New York, 1978).
27. Z.H. Levine, S.G. Louie, *Phys. Rev. B* **25**, 6310 (1982)
28. J.D. Fuhr et al., *Phys. Rev. B* **57**, 9329 (1998)
29. J.E. Miraglia, M.S. Gravielle, *Phys. Rev. A* **78**, 052705
 (2008)
30. J.E. Miraglia, M.S. Gravielle, *Phys. Rev. A* **81**, 042709
 (2010)
31. J.E. Miraglia, *Phys. Rev. A* **79**, 022708 (2008)
32. U. Kadhane, C.C. Montanar, L. Tribedi, *J. Phys. B* **36**,
 3043 (2003)
33. C.C. Montanari, J.E. Miraglia, *J. Phys. B* **47**, 015201
 (2014)
34. C.C. Montanari, J.E. Miraglia, *AIP Conf. Proc.* **1525**, 259
 (2013)
35. C.C. Montanari et al., *Phys. Rev. A* **75**, 022903 (2007)
36. C.C. Montanari, J.E. Miraglia, M. Behar, P.F. Duarte,
 N.R. Arista, J.C. Eckardt, G.H. Lantschner, *Phys. Rev. A*
77, 042901 (2008)
37. E. Clementi, C. Roetti, *At. Data Nucl. Data Tables* **14**,
 177 (1974)
38. G. Schiwietz, P.L. Grande, *Nucl. Instrum. Meth. B* **175**,
 175 (2001), CasP code, available online in [http://www.](http://www.casp-program.org/)
[casp-program.org/](http://www.casp-program.org/)
39. J.F. Ziegler, J.P. Biersack, U. Littmark, *The stopping and*
Range of ions in solids (Pergamon Press, 1985)
40. C. Schmitt, J. LaVerne, D. Robertson, M. Bowers, W. Lu,
 P. Collon, *Phys. Rev. A* **80** 052711 (2009)
41. C. Schmitt, J. LaVerne, D. Robertson, M. Bowers, W.
 Lu, P. Collon, *Nucl. Instrum. Meth. Phys. Res. B* **268** 1551
 (2010)
42. C. Schmitt, J. LaVerne, D. Robertson, M. Bowers, W. Lu,
 P. Collon, *Nucl. Instrum. Meth. Phys. Res. B* **269**, 721 (2011)
43. R.N. Sagaidak, V.K. Utyonkov, S.N. Dmitriev, *Nucl.*
Instrum. Meth. B **365**, 447 (2015)
44. P. Sigmund, A. Schinner, *Eur. Phys. J. D* **68**, 318 (2014)
45. P. Sigmund, A Schinner, *Nucl. Instrum. Meth. Phys. Res.*
B (2016), in press, DOI:10.1016/j.nimb.2015.12.041
46. N. Troullier, J.L. Martins, *Phys. Rev. B* **43**, 1993 (1991)
47. J.P. Perdew, K. Burke, M. Ernzerhof, *Phys. Rev. Lett.* **77**,
 3865 (1996)
48. *CRC Handbook of Chemistry and Physics*, edited by D.R.
 Lide, 89th edn. (CRC Press, Boca Raton, 2009)

- 1 49. H.K. Kim, S.H. Han, T.Y. Seong, W.K. Choi, J. Electrochem. Soc. **148**, G114 (2001) 17
2
3 50. A. Schleife, C. Rödl, F. Fuchs, J. Furthmüller, F. Bechstedt, Phys. Rev. B **80**, 035112 (2009) 18
4
5 51. A. Mang, K. Reimann, St. Rübenacke, Solid State Commun. **94**, 251 (1995) 19
6
7 52. V. Kumar, R.G. Singh, L.P. Purohit, F. Singh, Adv. Mat. Lett. **4**, 423 (2013) 20
8
9 53. R. Kumar, M.C. Mishra, B.K. Sharma, V. Vyas, G. Sharma, Electron. Mater. Lett. **9**, 19 (2013) 21
10
11 54. J.C. Aguiar, D. Mitnik, H.O. Di Rocco, J. Phys. Chem. Solids **83**, 64 (2015) 22
12
13 55. M. Vos, Nucl. Instrum. Meth. Phys. Res. B **366**, 6 (2016) 23
14
15 56. Bondiaux et al., Nucl. Instrum. Meth **168**, 29 (1980) 24
16
17 57. G. Schiwietz, P.L. Grande, Nucl. Instrum. Meth. Phys. Res. B **153**, 1 (1999) 25
18
19 58. G. Schiwietz, P.L. Grande, Nucl. Instrum. Meth. B **273**, 1 (2012) 26
20
21 59. G. Schiwietz, P.L. Grande, Phys. Rev. A **84**, 052703 (2011) 27
22
23 60. N. Bohr, Philos. Mag. **30**, 581 (1915) 28
24
25 61. A.F. Lifschitz, N.R. Arista, Phys. Rev. A **69**, 012902 (2004) 29
26
27 62. P. Sigmund, Particle Penetration and Radiation Effects, *Penetration of atomic and molecular ions* (Springer, Switzerland, 2014), Vol. 2 30
28
29 63. W.E. Lamb, Phys. Rev. **58**, 696 (1940) 31
30
31 64. H.D. Betz, Rev. Mod. Phys. **44**, 465 (1972)
65. K.X. To, R. Drouin, Nucl. Instrum. Meth. **160**, 461 (1978)
66. A. Itoh, H. Tsuchida, T. Majima, A. Yogo, A. Ogawa, Nucl. Instrum. Meth. Phys. Res. B **159**, 22 (1999)